

Modeling and Comparison of In-Field Critical Current Density Anisotropy in High-Temperature Superconducting (HTS) Coated Conductors

Di Hu, *Student Member, IEEE*, Mark D. Ainslie, *Member, IEEE*, Mark J. Raine, Damian P. Hampshire, and Jin Zou, *Student Member, IEEE*

(Invited Paper)

Abstract—The development of high-temperature superconducting (HTS) wires is now at a stage where long lengths of high quality are commercially available, and of these, (Re)BCO coated conductors show the most promise for practical applications. One of the most crucial aspects of coil and device modeling is providing accurate data for the anisotropy of the critical current density $J_c(B, \theta)$ of the superconductor. In this paper, the in-field critical current density characteristics $J_c(B, \theta)$ of two commercial HTS coated conductor samples are experimentally measured, and based on these data, an engineering formula is introduced to represent this electromagnetic behavior as the input data for numerical modeling. However, due to the complex nature of this behavior and the large number of variables involved, the computational speed of the model can be extremely slow. Therefore, a two-variable direct interpolation method is introduced, which completely avoids any complex data fitting for $J_c(B, \theta)$ and expresses the anisotropic behavior in the model directly and accurately with a significant improvement in computational speed. The two techniques are validated and compared using numerical models based on the H-formulation by calculating the self-field and in-field dc critical currents and the ac loss for a single coated conductor.

Index Terms—AC loss, critical current density (superconductivity), finite-element analysis, high-temperature superconductors, numerical analysis.

I. INTRODUCTION

RECENTLY, the processing of high temperature superconducting (HTS) wires has developed such that long lengths of high quality are available commercially, and of these, (RE)BCO coated conductors show the most promise for practical applications. The most significant characteristic of a superconductor for practical superconducting devices is the

maximum electrical transport current density it can maintain without resistance, or its critical current density, J_c . The maximum allowable current of HTS tapes/coils determines their safe operating margin, and in an HTS electric machine, for example, determines the volume and power density of the machine [1]–[3]. It is also expected that these materials could be exploited at 77 K, the boiling point of liquid nitrogen. However, these materials have presented a number of technical challenges for scientists and engineers alike, including grain boundaries and flux pinning, and the structural anisotropy, and therefore have a complex anisotropic J_c [4]–[7].

One of the most crucial aspects of coil and device modeling is providing accurate data for the anisotropy or angular dependence of the critical current density $J_c(B, \theta)$ for the superconductor. If this behavior is known in detail, it is possible to accurately predict the critical current and AC loss of coils and other devices. There are two methods—data fitting and interpolation—to include the experimental data of the anisotropic properties of a superconducting wire. Using data fitting, the authors in [8] develop an elliptical fitting function for this purpose. In [5], [6], the authors develop a method to describe a more complex $J_c(B, \theta)$ with 11 parameters at low magnetic fields (less than 0.21 T). In [9], the authors develop an alternative method to combine mathematical functions and a one-variable interpolation to achieve a fitting of a complex $J_c(B, \theta)$.

We are currently investigating the design of an all-superconducting axial flux-type electric machine using HTS materials in both bulk and wire forms [7], [10] and evaluating the performance of test HTS coils for this. As a starting point, this involves carrying out the measurement of the in-field critical current density properties of commercial HTS coated conductor. The experimental data for the modeling in this work comes from two short samples, measured at 77 K, from longer spools of wire (approximately 20 m) manufactured by SuperPower¹ and used to wind the test coils. Firstly, the basic properties and trends of the experimental data for these two samples are described. Based on these two data sets, we developed a method for data fitting and interpolation separately. For the data fitting, we develop an engineering formula to

Manuscript received August 31, 2015; accepted January 17, 2016. Date of publication January 25, 2016; date of current version March 11, 2016. This work was supported in part by a Henan International Cooperation Grant, China: 144300510014. The work of D. Hu and J. Zou was supported in part by Churchill College, the China Scholarship Council, and the Cambridge Commonwealth, European, and International Trust. The work of M. D. Ainslie was supported by a Royal Academy of Engineering Research Fellowship.

D. Hu, M. D. Ainslie, and J. Zou are with the Bulk Superconductivity Group, Department of Engineering, University of Cambridge, Cambridge CB2 1PZ, U.K. (e-mail: dh455@cam.ac.uk).

M. J. Raine and D. P. Hampshire are with the Department of Physics, University of Durham, Durham DH1 3LE, U.K.

Color versions of one or more of the figures in this paper are available online at <http://ieeexplore.ieee.org>.

Digital Object Identifier 10.1109/TASC.2016.2521585

¹SuperPower, Inc. [Online]. Available: <http://www.superpower-in.com>

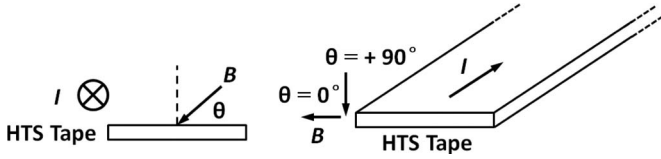


Fig. 1. Definition of the angular in-field dependence of the critical current density $J_c(B, \theta)$.

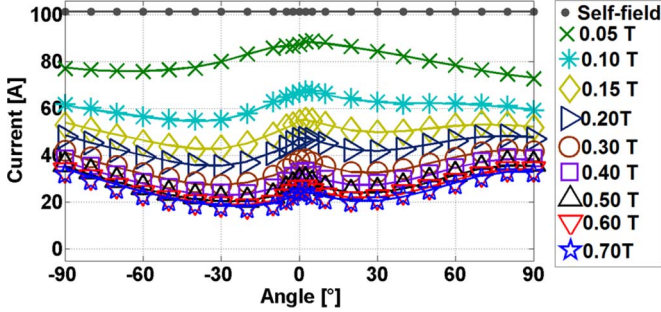


Fig. 2. Comparison of the experimental (symbols) and numerical data fitting (solid lines) for the angular in-field dependence of the critical current density $J_c(B, \theta)$ for sample SP1.

reproduce the measurements accurately from 0 T to 0.7 T. For the interpolation, we develop a two-variable direct interpolation to include $J_c(B, \theta)$ completely and directly. This is a simple and direct method, which avoids any complex data fitting and mathematical calculations.

To validate these models, numerical analyses are carried out using the H -formulation implemented in the commercial software package, Comsol Multiphysics 4.3a.² The numerical results for the self-field and in-field DC critical current and ac loss of a single wire are compared in detail, and a comparison of the computational times required for each method is made.

II. EXPERIMENTAL DATA ANALYSIS

Both samples are SuperPower's SCS4050-AP coated conductor¹ and labeled as SP1 and SP2. To measure the critical current, each sample was cooled to 77 K by submersion in a liquid nitrogen Dewar. The applied field was provided by using a conventional iron-cored, water-cooled electromagnet. The angular dependence of the in-field critical current of the sample $J_c(B, \theta)$ is defined as shown in Fig. 1, where the bottom surface is the substrate side. A voltage criterion of $E_0 = 1 \mu\text{V}/\text{cm}$ is used to define the critical current. The precision of the rotation angle for the applied field is 10° , with more precise angles around $\theta = 0^\circ$.

The experimental results for SP1 and SP2 are shown in Figs. 2 and 3, respectively. The spool including SP2 was used in the triangular, epoxy-impregnated coil presented in [7]. For both samples, the magnitude of the applied field was varied from 0 to 0.7 T in 0.05–0.1 T increments. The symbols in Figs. 2 and 3 represent the measured experimental results and the solid lines represent the numerical data fitting/interpolation.

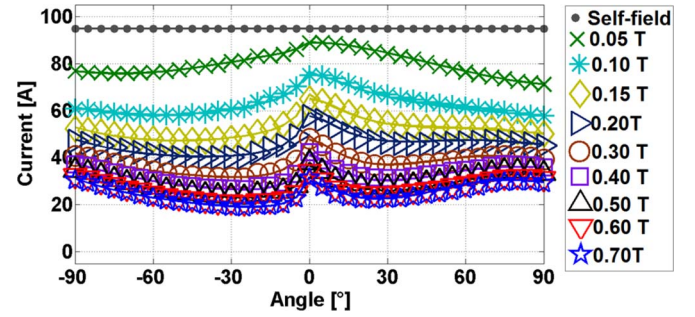


Fig. 3. Comparison of the experimental (symbols) and numerical data fitting (solid lines) for the angular in-field dependence of the critical current density $J_c(B, \theta)$ for sample SP2.

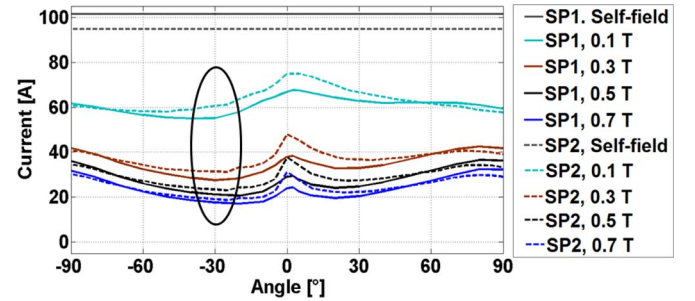


Fig. 4. Comparison of the experimental data for SP1 (solid lines) and SP2 (dashed line) for self-field and applied fields of 0.1, 0.3, 0.5, and 0.7 T.

It is interesting to compare the anisotropic properties of these two short samples. Fig. 4 shows a comparison of the measured data in self-field, and applied fields of 0.1 T, 0.3 T, 0.5 T and 0.7 T. Based on Fig. 4, it can be seen that the general trends of the curves, related to the manufacturing process and pinning, for the two samples are quite similar. There are three peaks at approximately 0° (parallel to the tape face) and $\pm 90^\circ$ (perpendicular to the tape face) for most cases. The minimum critical current occurs at approximately -30° and asymmetric tape behavior is observed between superconducting layer/substrate field directions.

Considering these similar trends in the two samples, an engineering formula can be developed for data fitting to input these data into the numerical model. For the data fitting, the basic form of the equation used is described by (1).

$$I_c(B, \theta) = \frac{I_{c0}}{\left(1 + B \sqrt{v(B, \theta)^2 \cos^2 \theta + u(B, \theta)^2 \sin^2 \theta} / B_0\right)^\beta} \quad (1)$$

where I_{c0} is the self-field critical current, B_0 and β are constants that depend on the material. Coefficients u and v are functions of the applied field magnitude B and field angle θ , and u and v are described by (2) and (3), respectively.

$$u(B, \theta) = b(B) \cos \theta + c(B)\theta + d(B) \quad (2)$$

$$v(B, \theta)^2 = a(B)^2, \text{ when } \theta \geq 0$$

$$v(B, \theta)^2 = |f(B)(\theta - \theta_0) \exp(g(B)\theta)|, \text{ when } \theta < 0 \quad (3)$$

²COMSOL, Inc. [Online]. Available: <http://www.comsol.com>

where $a - d$, f , and g are the functions of the applied field magnitude B , and θ_0 is a constant, which again depends on the material.

For SP1, we find $B_0 = 0.319$, $\beta = 2.405$, $I_{c0} = 101.4$, and $\theta_0 = 5$. Because of the asymmetric tape behavior, the functions of $a - d$, f , g should be considered separately when $\theta \geq 0$ and $\theta < 0$.

For $\theta \geq 0$:

$$a(B) = 0.7174 \exp(-0.9624B) - 1.567 \exp(-32.3B) \quad (4)$$

$$b(B) = -3.606 \exp(-1.001B) + 5.353 \exp(-12.93B) \quad (5)$$

$$c(B) = -3.509 \exp(-0.981B) + 5.818 \exp(-13.41B) \quad (6)$$

$$d(B) = 6.139 \exp(-1.002B) - 8.715 \exp(-13.96B) \quad (7)$$

For $\theta < 0$:

$$b(B) = 5.087 \exp(-1.372B) - 21.69 \exp(-37.35B) \quad (8)$$

$$c(B) = -5.593 \exp(-1.349B) + 20.09 \exp(-34.71B) \quad (9)$$

$$d(B) = -9.557 \exp(-1.366B) + 33.77 \exp(-36.22B) \quad (10)$$

$$f(B) = 6.286 \exp(-2.149B) - 15.94 \exp(-29.13B) \quad (11)$$

$$g(B) = 8.19 \exp(-1.81B) + 1.004 \exp(1.519B) \quad (12)$$

Based on equations (1)–(12), the data is fit for SP1 as shown in Fig. 2. It can be seen that our data fitting describes the experiment $J_c(B, \theta)$ data very well from self-field up to 0.7 T.

For SP2, we find $B_0 = 0.5$, $\beta = 1.446$, $I_{c0} = 94.7$, and $\theta_0 = 2.7$.

For $\theta \geq 0$:

$$a(B) = 1.15 \exp(-0.4108B) - 1.831 \exp(-19.68B) \quad (13)$$

$$b(B) = -1.526 \exp(1.625B) + 5.557 \ln(B + 10^{-5}) + 28.27 \exp(-9.14B) \quad (14)$$

$$c(B) = -8.954 \exp(-0.4397B) + 15.33 \exp(-10.36B) \quad (15)$$

$$d(B) = 15.61 \exp(-0.4722B) - 23.38 \exp(-10.77B) \quad (16)$$

For $\theta < 0$:

$$b(B) = 4.997 \exp(-0.596B) - 12.17 \exp(-11.24B) \quad (17)$$

$$c(B) = -6.042 \exp(-0.547B) + 13.88 \exp(-12.63B) \quad (18)$$

$$d(B) = -10.97 \exp(-0.5825B) + 22.62 \exp(-13.62B) \quad (19)$$

$$f(B) = 26.25 \exp(-0.9123B) - 41.28 \exp(-13.54B) \quad (20)$$

$$g(B) = 4.046 \sin(1.882B) + 54.94B \exp(-8.025B) \quad (21)$$

Based on equations (13)–(21), the data is fit for SP2 as shown in Fig. 3, which again matches very well.

From the basic form of the formulae (1)–(3), the specific parameters can be obtained by using a Matlab fit. Let us consider SP2 as an example. Firstly, $I_{c0} = 94.7$ A can be obtained

directly, and then by using a Matlab fit for the data at relatively low magnetic fields (e.g., 0.05 T, 0.1 T, and 0.15 T), the constant coefficients B_0 , θ_0 and β can be obtained. Next, by using a Matlab fit for all the experimental data, the other coefficients $a - d$, f , g can be obtained by trial and error. Based on our results, most of the coefficients $a - d$, f , g can be described in the form $m_1 \exp(n_1) + m_2 \exp(n_2)$.

Alternatively, an interpolation function can be used to describe the relationship between these coefficients and the applied field B . The two-variable direct interpolation method proposed here is a simpler and more direct method, similar to a look-up table. All of the experimental data can be input as a single function, with two input variables B and θ , and one output variable, the critical current density J_c , using a direct interpolation, which is available in Comsol. This significantly simplifies the process, and as shown later, dramatically improves the computational time required. A similar kind of interpolation, using one variable, has been applied in [11] for modeling the thermal properties of bulk MgB₂ superconductors.

Both the data fitting and two-variable direct interpolation are valid and accurate methods to include the experimental data in the model. However, accurate data fitting of complex $J_c(B, \theta)$ behavior like this needs complicated mathematical functions.

III. MODELING AND SIMULATION

Now that the two methods to include the experimental data have been defined, we should consider the accuracy of and computational time required when used in a numerical model. A 2D infinitely long model [12]–[15] is used to investigate the electromagnetic properties of a single tape, based on the \mathbf{H} -formulation [12], [16]–[18]. The width of the tape is 4 mm and the thickness of the superconducting layer is 1 μm . The tape is surrounded by an air sub-domain. The real thickness and width are modeled by the finite element method using Comsol. A mapped mesh is used in the superconducting layer to decrease the number of mesh elements [19] and a free triangular mesh is used in the air sub-domain. Linear, curl-conforming elements are employed for the entire model.

Similar to previous studies [12]–[15], [18]–[21] the governing equations are derived from Maxwell's equations: Faraday's law (22) and Ampere's law (23).

$$\nabla \times \mathbf{E} + d\mathbf{B}/dt = \nabla \times \mathbf{E} + d(\mu_0\mu_r\mathbf{H})/dt = 0 \quad (22)$$

$$\nabla \times \mathbf{H} = \mathbf{J} \quad (23)$$

where \mathbf{H} represents the magnetic field strength components, \mathbf{J} represents the current density and \mathbf{E} represents the electric field. μ_0 is the permeability of free space, and for the superconducting layer and air, the relative permeability is simply $\mu_r = 1$. In the 2D infinitely long model, $\mathbf{H} = [H_x, H_y]$, $\mathbf{J} = [J_z]$, $\mathbf{E} = [E_z]$.

It is assumed that electric field E_z is parallel to the current density J_z [12]–[15], [18]–[21] and the electrical properties of the superconductor are modeled by the E-J power law [22],

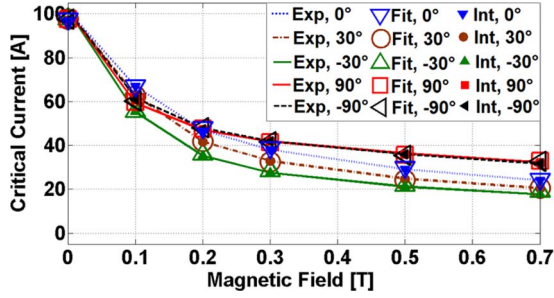


Fig. 5. Comparison of experimental results (lines), simulation results with data fitting (open symbols), and simulation results with the two-variable interpolation (closed symbols) for sample SP1.

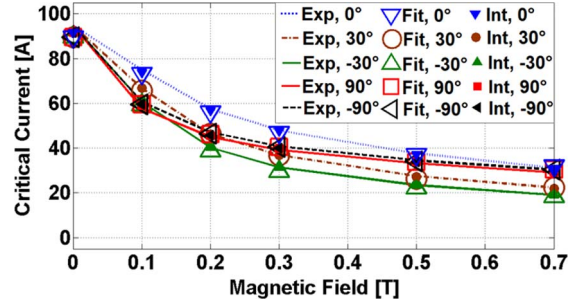


Fig. 6. Comparison of experimental results (lines), simulation results with data fitting (open symbols), and simulation results with the two-variable interpolation (closed symbols) for sample SP2.

in (24). The relationship between the critical current density $J_c(B, \theta)$ and the critical current $I_c(B, \theta)$ is given by (25).

$$\mathbf{E} = \left(\frac{E_0}{J_c(B, \theta)} \right) \left(\frac{|\mathbf{J}|}{|J_c(B, \theta)|} \right)^{n-1} \mathbf{J} \quad (24)$$

$$J_c(B, \theta) = \frac{I_c(B, \theta)}{S} \quad (25)$$

where E_0 is the characteristic electric field $1 \mu\text{V}/\text{cm}$ and S is the cross-section of the superconducting layer. For HTS materials, n is usually within the range of 5 (strong flux creep) and 50 (limiting value for HTS and LTS materials) [18], [22]. When $n > 20$, (24) becomes a good approximation of Bean's critical state model [24]. Therefore, in this paper, we assume $n = 21$.

The magnitude, B , and orientation, θ , of the magnetic field can be expressed by (26) and (27).

$$B = \sqrt{B_x^2 + B_y^2} \quad (26)$$

$$\theta = \arctan\left(\frac{B_y}{B_x}\right) \quad (27)$$

where $B_{x,y} = \mu_0 \mu_r H_{x,y}$.

For the non-superconducting air sub-domain surrounding the superconducting layer, a linear Ohm's law is considered, $\mathbf{E} = \rho \mathbf{J}$, where $\rho = 1 \Omega \cdot \text{m}$ is a specific, high constant resistivity for air.

Integral constraints are applied to the superconducting layer to represent the particular transport current flowing in the superconducting tape. A transport current I_s through the cross-section S of the tape is therefore described by (28) [20].

$$I_s = \int \mathbf{J} \cdot d\mathbf{S} \quad (28)$$

The calculation of the ac loss [J/m/cycle] of the superconducting tape in the 2D infinitely long model can be expressed as (29).

$$\text{AC loss} = \int_0^T \int \mathbf{E} \cdot \mathbf{J} dS dt \quad (29)$$

where T is the period of one cycle.

IV. RESULT AND DISCUSSION

A. In-Field DC Critical Current Calculation

A comparison of the numerical simulation results for the self-field and in-field DC critical currents for the short samples SP1 and SP2 using the data fitting and two-variable direct interpolation methods are shown in Figs. 5 and 6, respectively. Some particular angles of the applied magnetic field are chosen: 0° (parallel to the tape face), $\pm 30^\circ$ (roughly where the minimum I_c occurs) and $\pm 90^\circ$ (perpendicular to the tape face). Except for the method of including the experimental data for $J_c(B, \theta)$, all the settings for these models are the same.

Based on Figs. 5 and 6, it can be seen that our simulation results by data fitting and two-variable direct interpolation are consistent with the experimental results, so their accuracy is validated. There is a slight difference between the simulation and measurements in self-field (i.e., 0 T) because no correction is made for the effect of the self-field in the simulation (see [5], for example). However, these errors are no more than 5% for our cases and this is not considered too important since in most practical applications the magnetic field seen by the superconductor is usually much greater than the self-field, such as in HTS coils for electrical machines.

To assess the computational speed of the two methods, the time required to solve each set of model parameters for the data fitting and two-variable direct interpolation methods is shown in Table I. The simulations were carried out using a desktop computer with an Intel i7 3.20 GHz processor and 16 GB of memory. Table I shows the computational time for the models for the short sample SP1 at applied field angles of 0° , $\pm 30^\circ$, and $\pm 90^\circ$. Very similar results were observed for SP2, the results for which have been omitted here. DF represents the data fitting method; INT represents the two-variable direct interpolation method.

From Table I, it can be seen that the computational times for the two-variable direct interpolation are all of the same order for all cases and vary between 300 s to 679 s. For the data fitting method, the computational time varies greatly depending on the angle and magnitude of the applied field, but is significantly slower than the interpolation method, varying from around five times slower ($\pm 90^\circ$) up to over 100 times slower (0°). Hence, the two-variable direct interpolation is not only much faster, but much more consistent in terms of model convergence and solver time.

TABLE I
COMPUTATIONAL TIME REQUIRED TO CALCULATE THE IN-FIELD DC
CRITICAL CURRENT USING THE DATA FITTING AND TWO-VARIABLE
DIRECT INTERPOLATION METHODS FOR SHORT SAMPLE SP1
AT DIFFERENT APPLIED FIELD ANGLES. ALL VALUES
ARE GIVEN IN UNITS OF SECONDS (s)

APPLIED FIELD	0°		-30°		30°	
	DF	INT	DF	INT	DF	INT
0 T	1958	344	2245	375	2145	368
0.1 T	36878	355	20180	383	15077	438
0.2 T	44864	339	28568	432	25593	395
0.3 T	53764	338	37693	397	33684	448
0.5 T	62247	316	44341	679	40437	629
0.7 T	71665	586	50764	590	48837	620

APPLIED FIELD	-90°		90°	
	DF	INT	DF	INT
0 T	1780	337	2041	352
0.1 T	1834	398	2507	434
0.2 T	1695	412	2187	466
0.3 T	1675	433	2345	451
0.5 T	1655	387	2303	396
0.7 T	1476	348	2252	390

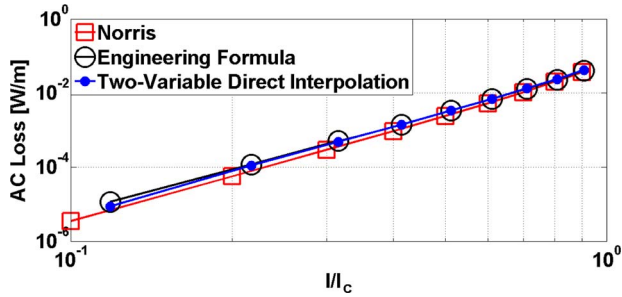


Fig. 7. Comparison of ac loss of sample SP1 by three methods.

B. AC Loss Calculation

Another important reason to include accurate experimental data for $J_c(B, \theta)$ is to calculate the ac loss of HTS tapes and coils. AC loss is an important problem for HTS devices exposed to a time-varying current or magnetic field, which can directly influence the refrigeration load and therefore decrease the overall device efficiency and increase the complexity of design [3].

To verify the model, the AC loss calculation of a single HTS tape in self-field is compared to Norris's analytical solution [25] for the engineering formula and the two-variable direct interpolation for a frequency of $f = 50$ Hz. The current is varied between $0.1 I_c$ and $0.95 I_c$ where I_c represents the self-field DC critical current of the tape. The ac loss results are shown in Figs. 7 and 8 for samples SP1 and SP2, respectively, and it can be seen that the ac loss calculation is consistent for both methods. The slight difference between the engineering formula/interpolation and Norris's analytical solution arises because Norris's analysis assumes a constant J_c and does not take into account the in-field behavior.

V. CONCLUSION

In this paper, the angular dependence of the critical current density for two samples of SuperPower's SCS4050-AP coated

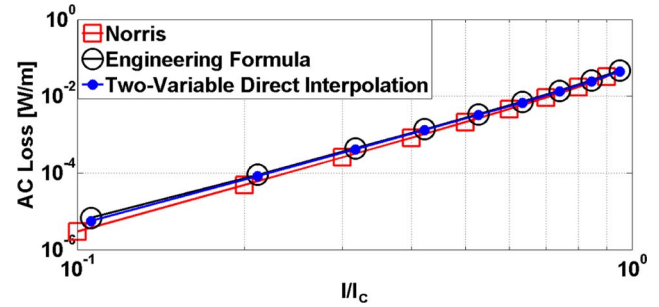


Fig. 8. Comparison of ac loss of sample SP2 by three methods.

conductor is measured and compared. Based on this experimental data, the asymmetric $J_c(B, \theta)$ behavior is input into numerical models using two methods: data fitting using an engineering formula, and a simpler and more direct method using a two-variable direct interpolation. The numerical models, which are based on the H -formulation and implemented in Comsol Multiphysics, are used to verify the effectiveness of the two methods to calculate the in-field DC critical current and the ac loss for a single tape. It is found that two methods are both accurate, but the two-variable direct interpolation is significantly faster than the data fitting method using an engineering formula, in some cases up to over 100 times faster. The direct interpolation method is therefore recommended as the best method to include anisotropic $J_c(B, \theta)$ behavior to model HTS coated conductors in finite element models to achieve accurate, effective and efficient results.

REFERENCES

- [1] T. Konishi, T. Nakamura, T. Nishimura, and N. Amemiya, "Analytic evaluation of HTS induction motor for electric rolling stock," *IEEE Trans. Appl. Supercond.*, vol. 21, no. 3, pp. 1123–1126, Jun. 2011.
- [2] M. Oomen *et al.*, "Manufacturing and test of 2G-HTS coils for rotating machines: Challenges, conductor requirements, realization," *Physica C*, vol. 482, pp. 111–118, Apr. 2012.
- [3] D. Hu, M. D. Ainslie, J. Zou, and D. A. Cardwell, "Numerical analysis of non-uniformities and anisotropy in high-temperature superconducting coils," *IEEE Trans. Appl. Supercond.*, vol. 25, no. 3, Jun. 2015, Art. ID 4900605.
- [4] V. Selvamaniyam *et al.*, "Enhanced and uniform in-field performance in long (Gd, Y)-Ba-Cu-O tapes with zirconium doping fabricated by metal-organic chemical vapor deposition," *Supercond. Sci. Technol.*, vol. 23, Jan. 2010, Art. ID 014014.
- [5] E. Pardo, M. Vojenciak, F. Gomory, and J. Souc, "Low-magnetic-field dependence and anisotropy of the critical current density in coated conductors," *Supercond. Sci. Technol.*, vol. 24, Apr. 2011, Art. ID 065007.
- [6] F. Gomory *et al.*, "AC loss in pancake coil made from 12 mm wide REBCO tape," *IEEE Trans. Appl. Supercond.*, vol. 23, no. 3, Jun. 2013, Art. ID 5900406.
- [7] D. Hu *et al.*, "DC characterization and 3D modelling of a triangular, epoxy-impregnated high temperature superconducting coil," *Supercond. Sci. Technol.*, vol. 28, no. 6, Apr. 2015, Art. ID 065011.
- [8] L. Rostila *et al.*, "How to determine critical current density in YBCO tapes from voltage-current measurements at low magnetic field," *Supercond. Sci. Technol.*, vol. 20, pp. 1097–1100, Sep. 2007.
- [9] M. Zhang *et al.*, "Study of second generation, high-temperature superconducting coils, Determination of critical current," *J. Appl. Phys.*, vol. 111, Apr. 2012, Art. ID 083902.
- [10] M. D. Ainslie *et al.*, "Design and market considerations for axial flux superconducting electric machine design," *J. Phys., Conf. Ser.*, vol. 507, 2014, Art. ID 032002.
- [11] J. Zou *et al.*, "Numerical modelling and comparison of MgB2 bulks fabricated by HIP and infiltration growth," *Supercond. Sci. Technol.*, vol. 28, no. 7, Jul. 2015, Art. ID 075009.

- [12] R. Brambilla, F. Grilli, and L. Martini, "Development of an edge-element model for AC loss computation of high temperature superconductors," *Supercond. Sci. Technol.*, vol. 20, no. 1, pp. 16–24, Jan. 2007.
- [13] M. D. Ainslie, T. J. Flack, Z. Hong, and T. A. Coombs, "Comparison of first- and second-order 2D finite element models for calculating AC loss in high temperature superconductor coated conductors," *Int. J. Comput. Math. Elect. Electron. Eng.*, vol. 30, no. 2, pp. 762–774, 2011.
- [14] M. D. Ainslie *et al.*, "Modeling and electrical measurement of transport AC loss in HTS-based superconducting coils for electric machines," *IEEE Trans. Appl. Supercond.*, vol. 21, no. 3, pp. 3265–3268, Jun. 2011.
- [15] M. D. Ainslie, T. J. Flack, and A. M. Campbell, "Calculating transport AC losses in stacks of high temperature superconductor coated conductors with magnetic substrates using FEM," *Physica C*, vol. 472, no. 1, pp. 50–56, Jan. 2012.
- [16] R. Pecher, M. D. McCulloch, S. J. Chapman, L. Progozhin, and C. M. Elliott, "3D-modelling of bulk type-II superconductors using unconstrained H-formulation," in *Proc. 6th Eur. Conf. Appl. Supercond.*, Sep. 2003, pp. 1–11.
- [17] K. Kajikawa, T. Hayashi, R. Yoshida, M. Iwakuma, and K. Funaki, "Numerical evaluation of AC losses in HTS wires with 2D FEM formulated by self magnetic field," *IEEE Trans. Appl. Supercond.*, vol. 13, no. 2, pp. 3630–3633, Jun. 2003.
- [18] Z. Hong, A. M. Campbell, and T. A. Coombs, "Numerical solution of critical state in superconductivity by finite element software," *Supercond. Sci. Technol.*, vol. 19, no. 12, pp. 1246–1252, Dec. 2006.
- [19] M. D. Ainslie *et al.*, "An improved FEM model for computing transport AC loss in coils made of RABiTS YBCO coated conductors for electric machines," *Supercond. Sci. Technol.*, vol. 24, no. 4, Apr. 2011, Art. ID 045005.
- [20] D. Hu, M. D. Ainslie, J. Zou, and D. A. Cardwell, "3D modelling of all-superconducting synchronous electric machine by the finite element method," in *Proc. COMSOL Conf.*, Cambridge, U.K., Sep. 2014, pp. 1–7.
- [21] M. D. Ainslie, D. Hu, J. Zou, and D. A. Cardwell, "Simulating the in-field AC and DC performance of high- temperature superconducting coils," *IEEE Trans. Appl. Supercond.*, vol. 25, no. 3, Jun. 2015, Art. ID 4602305.
- [22] C. J. G. Plummer and J. E. Evetts, "Dependence of the shape of the resistive transition on composite homogeneity in multifilamentary wires," *IEEE Trans. Magn.*, vol. MAG-23, no. 2, pp. 1179–1182, Mar. 1987.
- [23] J. Rhyner, "Magnetic properties and AC-losses of superconductors with power law current–voltage characteristics," *Physica C*, vol. 212, no. 3/4, pp. 292–300, Jul. 1993.
- [24] F. Grilli *et al.*, "Finite-element method modeling of superconductors: From 2-D to 3-D," *IEEE Trans. Appl. Supercond.*, vol. 15, no. 1, pp. 17–25, Mar. 2005.
- [25] W. T. Norris, "Calculation of hysteresis loss in hard superconductors carrying ac: Isolated conductors and edges of thin sheets," *J. Phys. D, Appl. Phys.*, vol. 3, pp. 489–507, 1969.